Homogenization of Pseudomonas aeruginosa PAO1 biofilms from high-resolution visualization by freeze substitution

T. Guélon, R.C. Hunter, Jean-Denis Mathias, G. Deffuant

Author-produced version of the paper published in Biotechnology and Bioengineering, vol.110, n°5,1405-1418.
Original version available from doi : 10.1002/bit.24805, http://onlinelibrary.wiley.com

Homogenization of *Pseudomonas aeruginosa* PAO1 biofilms visualized by freeze-substitution electron microscopy

T. Guélon[1*], R.C. Hunter[2], J.D. Mathias[1], G. Deffuant[1]

[1] Irstea - LISC (Laboratoire d'Ingénierie pour les Systèmes Complexes) Clermont-Ferrand, 24 avenue des Landais BP 50085 63172 Aubière Cedex 1 – France.

[2] Howard Hughes Medical Institute, Division of Biology, California Institute of Technology Pasadena, CA 91125.

[*] Corresponding author, Phone: +33 473440683, E-mail address: thomas.guelon@irstea.fr (Thomas Guélon)
Address : Irstea - LISC (Laboratoire d'Ingénierie pour les Systèmes Complexes) Clermont-Ferrand, 24 avenue des Landais BP 50085 63172 Aubière Cedex 1 – France.

Running title : Homogenization of biofilms mechanical properties

Abstract:

A knowledge of the mechanical properties of bacterial biofilms is required to more fully understand the processes of biofilm formation such as initial adhesion or detachment. The main contribution of this paper is to demonstrate the use of homogenization techniques to compute mechanical parameters of *Pseudomonas aeruginosa* PAO1 biofilms. For this purpose, homogenization techniques are used to analyze freeze substitution electron micrographs of the biofilm cross-sections. The concept of a representative volume element and the study about his representativeness allows us to determine the optimal size in order to analyse these biofilm images. Results demonstrate significant heterogeneities with respect to stiffness and these can be explained by varying cell density distribution throughout the bacterial biofilms. These stiffness variations lead to different mechanical properties along the height of the biofilm. Moreover, a numerical shear stress test shows the impact of these heterogeneities on the detachment process. Several modes of detachment are highlighted according to the local strain energy in the different parts of the biofilm. Knowing where, and how, a biofilm may detach will allow better prediction of accumulation and biomass detachment.

Keywords: homogenization technique; mechanical properties; freeze-substitution electron microscopy; bacterial biofilms; detachment process.

1 Introduction

Bacteria predominantly live in surface-associated communities called biofilms which develop at any interface that is suitable for microbial growth (Costerton *et al.* 1995). Important examples where biofilms occur are riverbeds, plant leaves, waste water treatment facilities (Woolard and Irvine 1994; Wagner and Loy 2002), soil, sites of biocorrosion (Beech and Sunner 2004), (Coetser and Cloete 2005), sewage pipelines, bioreactors (Godon *et al.* 1997), and several sites throughout the human host (Socransky and Haffajee 2002; Marsh and Bradshaw 1995). Bacterial biofilms can be beneficially used in the wastewater treatment process (Woolard and Irvine 1994; Wagner and Loy 2002) but they can also be harmful in many industrial processes (such as water distribution pipelines) and in infectious disease. In any case, favouring the maintenance or removal of a biofilm community requires a better understanding and control of its mechanical properties. Indeed, the mechanical properties of biofilms determine biofilm deformation, failure and detachment in response to mechanical forces.

Characterizing the mechanical properties of biofilm communities is therefore an important scientific and economic issue. For example, techniques that use mechanical forces in the absence of hydrodynamics include micro-cantilevers (Poppele and Hozalski 2003; Aggarwal and Hozalski 2010; Aggarwal *et al.* 2010), centrifugation methods (Ohashi and Harada 1994a, 1996), indenters (Cense *et al.* 2006), and T-shaped probes (Chen *et al.* 1998, 2005) in order to pull the biofilm. Other methods use hydrodynamic loadings (exposure of biofilms to a fluid flow) including flow cell methods (Stoodley *et al.* 1999a, b, 2001, 2002; Mathias and Stoodley 2009) or Couette-Taylor reactors (Coufort *et al.* 2007; Rochex *et al.* 2008). This range of studies highlights different mechanical behaviours, some of which report a linear behaviour of the biofilm (Korstgens *et al.* 2001; Mathias and Stoodley 2009). Generally, bacterial biofilms present a linear behaviour when they are submitted to low loadings, and their mechanical behaviour can be described in the elasticity framework. However, biofilms can also demonstrate time-dependent properties of viscoelastic materials with a relaxation time on the order of minutes (Klapper *et al.* 2002; Cense *et al.* 2006; Lau *et al.* 2009). In order to further understand these behaviours, various numerical models have been developed, including sensitivity analyses on the parameters of a generalized Maxwell model (Klapper *et al.* 2002). A detailed review presents experimental devices and mechanical characterization of bacterial biofilms (Guélon *et al.*, 2011).

These mechanical behaviours directly depend on the microstructure of the biofilm such as the porosity or the bacterial density. To understand these contributions in more detail, several experimental studies have investigated the heterogeneity of these parameters on sub-micron scales (DeBeer *et al.* 1994; DeBeer and Stoodley 1995). For example, confocal microscopy provides a non-invasive visualization of a biofilm in three-dimensions and has revealed a variety of spatial structures – including mushroom (Rieu *et al.* 2008; Allesen-Holm *et al.* 2006), complex, or labyrinth morphologies (Xavier *et al.* 2009). Moreover, innovative imaging methods

such as the freeze-substitution technique (Hunter and Beveridge 2005) can reveal structural details of a biofilm in its near-native state at much higher resolution than classical confocal studies. Regardless of observation techniques, many studies have suggested that biofilm spatial structures, on multiple scales, can have a drastic effect on mechanical properties.

However, the influence of microstructures on biofilm mechanics has seldom been addressed in the literature from a numerical point of view. A lot of environmental systems contain many spatial scales. The upscaling techniques such as the homogenization technique or the averaging theorem allow us to determine the macroscopic behaviour of a heterogeneous material from the knowledge of mechanical properties of each phase component and their spatial distribution. Numerical studies are mainly based on homogenization techniques in order to determine mechanical properties of various materials (Hashin, 1962; Aboudi 1991; Dormieux 2002). Indeed, the homogenization techniques are mainly used in the study of material behaviours. Moreover, in the field of bacterial biofilms, physical properties of biofilms have been highlighted with the averaging theorem (Wood and Whitaker 1998, 1999) or the homogenization techniques (Guélon *et al*. 2012), which both are used to determine the effective diffusion parameters of a biofilm. Some analytical models have also been developed in simple cases (Chang 1983). Moreover, some studies have investigated variations in mechanical properties of porous composite materials in order to calculate the Young's modulus. In these studies, bacterial biofilms are treated as porous composite materials with solid phases and voids (Laspidou *et al*. 2005; Laspidou and Aravas 2007).

In this study, we aim to characterize the influence of biofilm microstructure on its mechanical properties. We use freeze-substitution transmission electron microscopy for high-resolution imaging of the natural structure of *Pseudomonas aeruginosa* biofilms (Hunter and Beveridge 2005) and then use these images as the representative volume element (RVE) for homogenization techniques. We first analyse the impact of the bacteria spatial distribution throughout the biofilm in terms of mechanical properties. Then, an energetic criterion was used to determine the kind of detachment and the location where it is the most probable to occur.

2 Materials and Methods

2.1 Experimental techniques

P. aeruginosa PAO1 was used throughout this study and was obtained from J. S. Lam (University of Guelph) and was maintained on trypticase soy agar (TSA, Becton Dickinson). Planktonic cultures were grown in a dilute Trypticase soy broth medium (dTSB) at a concentration of 3 $g.l^{-1}$ (1/10th the recommended concentration) at room temperature to late-exponential phase. Cells were washed twice in 50 mM HEPES buffer and were then processed using freeze-substitution (Hunter and Beveridge 2005) as previously described.

Biofilms were cultivated in dTSB on sapphire disks (Al_2O_3) that were 50 µm thick and 1.4 mm in diameter (Leica Microsystems). Sapphire disks were placed in the lumen of silicone tubing (inner diameter of 1.57 mm) and the entire system was autoclaved prior to inoculation. Following attachment of cells to the sapphire disks, flow was resumed and the dTSB was pumped through at a constant rate of 0.1 $mL.min^{-1}$or 7 days. After 7 days of growth, flow was stopped and sterile forceps were used to remove the sapphire disks. We can note that no visible biomass was detached from the Sapphire discs during processing. Sapphire disks were then placed into flat specimen holders (Leica) that were 1.5 mm in diameter. Immediately prior to freezing, a 10% sucrose solution was placed over top of the biofilm to serve as a cryoprotectant. The sapphire disks were frozen using a Leica EM PACT high-pressure freezer. Once samples were frozen they were maintained under liquid nitrogen (-135°C).

Transmission electron microscopy was then used to image the obtained biofilms. Biofilms were thin sectioned on a Reichert-Jung Ultracut E ultramicrotome and visualized on a Philips CM10 transmission electron microscope operating at 80 kV under standard operating conditions.

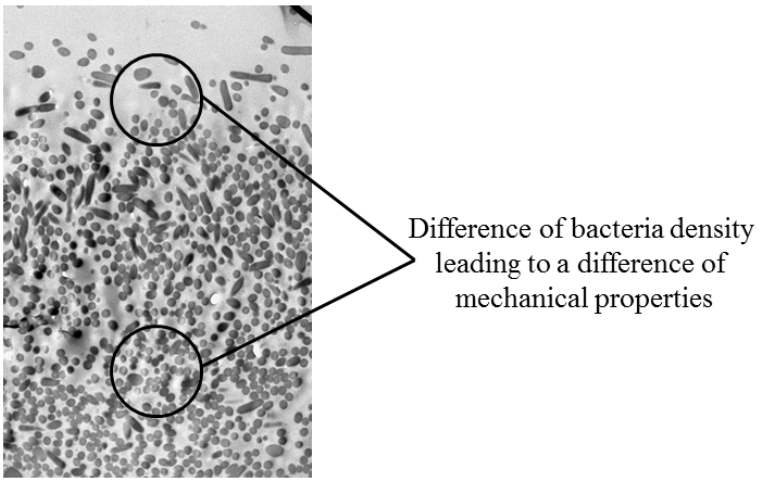

Figure 1: Experimental investigation of a *Pseudomonas aeruginosa* biofilm using freeze-substitution technique (Hunter and baveridge 2005). The density of bacteria changes following the location within the biofilm.

Intuitively, bacteria and their extracellular polymeric substances (EPS) have different mechanical properties. Moreover, as shown in Figure 1, the bacterial distribution is not the same at the top of the biofilm as it is at the bottom. These variations in spatial organization can lead to localized gradients. However, it is difficult to evaluate the effect of these properties on biofilm mechanics. In order to assess these heterogeneities and their influence on the mechanical properties of the biofilm, we apply homogenization procedures on experimental images of separate biofilms of *Pseudomonas aeruginosa* PAO1 (Figure 2). This experimental set up has

been chosen because it is a non-destructive experiment. It allows us to generate relevant experimental images with a high resolution where the bacteria spatial distribution can be clearly investigated.

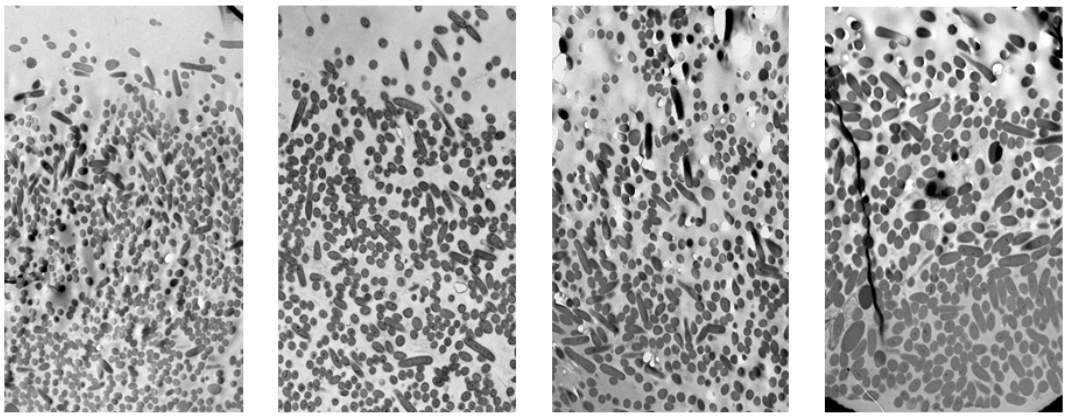

Image 1 Image 2 Image 3 Image 4

Figure 2: Experimental images of *Pseudomonas aeruginosa* visualized by freeze substitution electron microscopy. Homogenization method has been performed on these four experimental images.

2.2 Homogenization techniques

Biofilms investigated in this study are considered as a two-phase material: bacterial cells and their extracellular polymeric substances (EPS). At the microscopic scale, we assume that both components have a linear elastic isotropic behaviour:

$$\underline{\underline{\varepsilon}} = \frac{1+\nu}{E}\underline{\underline{\sigma}} - \frac{\nu}{E}Tr(\underline{\underline{\sigma}})\underline{\underline{I}} \qquad (1)$$

$\underline{\underline{\sigma}}$ and $\underline{\underline{\varepsilon}}$ are the classical stress and strain tensors. $Tr(\underline{\underline{\sigma}})$ corresponds to the trace of the matrix $\underline{\underline{\sigma}}$, *i.e.*, the sum of the elements on the diagonal, $\underline{\underline{I}}$ is the identity matrix. *E* corresponds to the Young's modulus or the stiffness and ν is the Poisson's ratio. These coefficients are denoted E_b and ν_b for the bacteria, and E_m, ν_m for the EPS. These values are then used to calculate the homogenized macroscopic values for the biofilm, denoted E_h and ν_h. The assumptions of linear elastic behaviour are based on previous studies of biofilm mechanical properties (Korstgens *et al.* 2001, Mathias et Stoodley 2009). Generally, bacterial biofilms present a linear behaviour when they are submitted to low loadings and their behaviour can be described in the elasticity

framework. It is important to note that, despite microrheological *in situ* measurements of biofilm "streamers" demonstrating a clear viscoelasticity (Stoodley *et al.* 1999, 2002), we assume that biofilms have a linear elastic isotropic behaviour. We use homogenization techniques based on a representative volume element to characterize their elastic properties.

2.3 Representative volume element (RVE)

Homogenization procedures have been often used to determine the behaviour of different materials (Hashin 1962; Mori and Tanaka 1973; Suquet 1997). Furthermore, they integrate complex behaviour in order to calculate equivalent properties. This is not possible with classical methods that consider an uniform distribution of the particles, such as the Hashin-Shtrikman bounds (Hashin and Shtrikman 1963). Here, we use a numerical homogenization procedure in which complex spatial structures and spatial heterogeneities are taken into account using a representative volume element (RVE). For this, it is necessary to have a large surface in order to be representative, which depends on the studied scale and properties under consideration. It is essential to perform convergence studies to determine the size of the RVE (Figure 3).

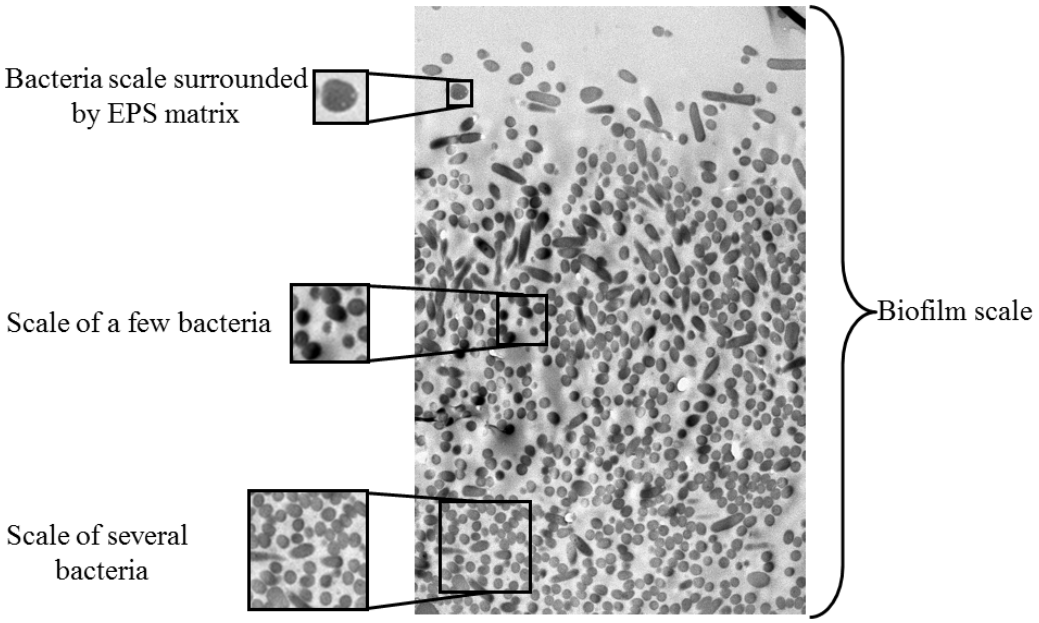

Figure 3: Selection of a representative volume element. We can clearly distinguish different scales from one bacteria to a cluster of bacteria.

Indeed, if the surface is too small, the RVE is not representative. If the surface is too large, heterogeneities become smoothed. Therefore, when the RVE is determined, we attempt to shift this RVE so as to calculate and map the corresponding mechanical properties. The size of the biofilm images is 60×45 µm² and each has been imported on Inkscape (inkscape.org). The resolution of the experimental image is 560×360 pixels and they have been converted in .dxf format. The sizes of the three other images are close to this resolution. We have adopted the thresholding process by brightness cutoff with a single path from biofilm images. It has been used to create binary images in order to export them on the Finite Element (FE) software Comsol. The Inkscape software uses the vectorization engine Potrace (potrace.sourceforge.net). The geometry is then meshed with 2D triangular elements with 6 nodes per element. The number of elements of the meshing changes according to the geometry of the RVE.

2.4 Energy-based technique

The aim of this section is to use energy-based technique in order to determine the mechanical properties of the equivalent system from the microscopic components of the system. This technique is based on the assumption that the strain energy in the biofilm (considered a two phase material - bacteria and EPS) is equivalent to the homogenized strain energy of an equivalent homogenous biofilm.

If we consider an isotropic elastic behaviour of the homogenized system (see results section 3.2), the homogenized strain energy W^{hom} writes:

$$W^{\hom} = \frac{E_h}{2(1-\nu_h^{\,2})}\varepsilon_{11}^2 + \frac{-\nu_h}{(1-\nu_h^{\,2})}\varepsilon_{11}\varepsilon_{22} + \frac{E_h}{2(1-\nu_h^{\,2})}\varepsilon_{22}^2 + \frac{E_h}{4(1+\nu_h)}\varepsilon_{12}^2 \qquad (2)$$

E_h and ν_h are the homogenized Young's modulus and the homogenized Poisson's ratio respectively. ε_{11}, ε_{12}, ε_{22} are the homogenized elements of the matrix $\underline{\underline{\varepsilon}}$.

Equation 2 has two unknowns, two mechanical tests are therefore required to determine these. The general approach developed in this study consists of simulating mechanical tests using FE software. We then compare the homogenized strain energy W^{hom} to the strain energy W^{num} of the real structure:

$$W^{num} = \frac{1}{2e}\int_S \underline{\underline{\sigma}} : \underline{\underline{\varepsilon}}\ \mathrm{ds} \qquad (3)$$

The FE tests give us two equations and therefore allows us to determine the homogenized parameters E_h and ν_h by the equality of Equations 2 and 3.

2.5 Mechanical tests

Identifying the Young's modulus E and the Poisson's ratio ν requires two mechanical tests, chosen for simplifying Equation 2. Here, an elementary cell is made of images described in section 2.1. An example of an elementary cell, exhibiting bacteria embedded in EPS is shown in Figure 4. Mechanical tests were performed using the FE software.

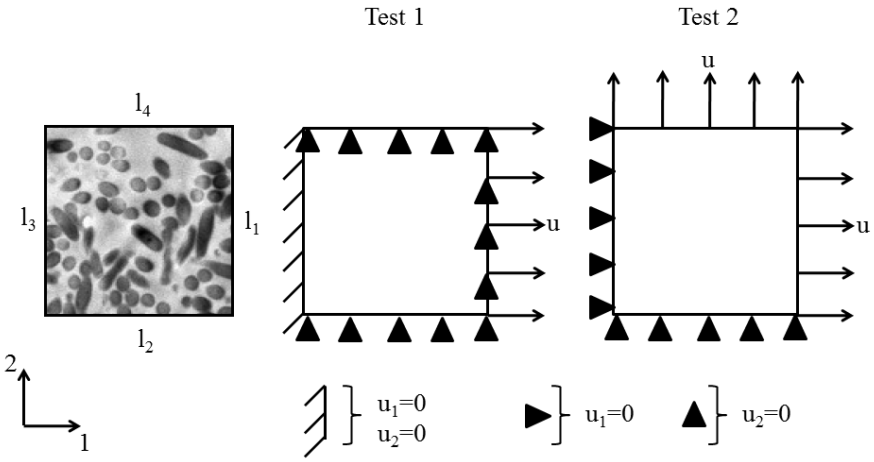

Figure 4: Elementary cell of bacterial biofilm. Boundary conditions are imposed on the different edges l_1, l_2, l_3 and l_4 of the considered RVE for tests 1 and 2.

The length of the cell side is denoted *l*. To carry out the numerical procedure, the elementary cell is supposed to be submitted to homogeneous strains ε^0 on the boundary ∂S using a linear displacement u^d. The local problem can be formalized as follows:

$$\begin{cases} div(\sigma(x)) = 0 \\ \sigma(x) = C(x) : \varepsilon(u(x)) \text{ in } S \\ u^d = \varepsilon^0 . x \text{ on } \partial S \end{cases} \quad (4)$$

Some relevant displacements u^d are imposed on ∂S that is to say on the four lines l_1, l_2, l_3 and l_4. Test 1 corresponds to a uniaxial tensile test and test 2 to a simple shear test. Figure 4 illustrates the boundary conditions chosen for both tests:

for test 1:

$$\begin{cases} u_1(l_1) = u \\ u_1(l_2) = u_1(l_4) = u \times x \\ u_1(l_3) = 0 \\ u_2(l_1) = u_2(l_2) = u_2(l_3) = u_2(l_4) = 0 \end{cases} \quad (5)$$

for test 2:

$$\begin{cases} u_1(l_1) = u \\ u_1(l_2) = u_1(l_4) = u \times x \\ u_1(l_3) = 0 \\ u_2(l_2) = 0 \\ u_2(l_1) = u_2(l_3) = u \times y \\ u_2(l_4) = u \end{cases} \tag{6}$$

where u is a constant.

u_1 and u_2 represent the displacements along the 1-direction and the 2-direction. The computation of the strain energy for these tests gives the following results:

for test 1:

$$W^{t1} = \frac{E_h}{2(1-\nu_h^{\,2})}(\frac{u}{l})^2 \tag{7}$$

for test 2:

$$W^{t2} = \frac{E_h}{(1-\nu_h)}(\frac{u}{l})^2 \tag{8}$$

Using Equations 7 and 8, the Young's modulus E_h and the Poisson's ratio ν_h of the homogenized model can be calculated:

$$\begin{cases} \nu_h = \dfrac{(W^{t2} - 2W^{t1})}{2W^{t1}} \\ E_h = \dfrac{W^{t2}(1-\nu_h)}{(\frac{u}{l})^2} \end{cases} \tag{9}$$

2.6 Analytical Solutions

Several theoretical models calculate effective elastic moduli in a two-phase media. The simplest model is the law of mixtures. The bounds of Voigt and Reuss are based on this law (Reuss 1929; Voigt 1889). These models are essentially based on the assumption of a uniform distribution of inclusions or fibers. The influence of the spatial structure is neglected in this type of model which constitutes a mean field approximation of the effective properties in the case of a uniform distribution. It is simply assumed that for the Reuss model, the stress is constant in both phases and, for the Voigt model, it is the strain which is constant.

Hashin and Shtrikman have later established a variational principle able to give more precise bounds on effective properties of the material by adding an assumption on the geometry: there is a continuous phase and a discontinuous one (Hashin and Shtrikman 1963; Hashin 1983). They have shown that the effective properties of a two-phase material are bounded by the following expressions where it is assumed that $G_1 < G_2$ and $K_1 < K_2$. In this section, the index 1 refers to the EPS matrix and the index 2 to the bacteria. We denoted ρ_i, the ratio between the area occupied by the *i*-phase and the total area.

We define the bounds of the shear modulus G as :

$$G^- = G_1 + \frac{\rho_2}{\frac{1}{(G_2 - G_1)} + \frac{6(K_1 + 2K_1)\rho_2}{5G_1(3K_1 + 4G_1)}} \tag{10}$$

$$G^+ = G_2 + \frac{\rho_1}{\frac{1}{(G_1 - G_2)} + \frac{6(K_2 + 2K_2)\rho_2}{5G_2(3K_2 + 4G_2)}} \tag{11}$$

We define the bounds of the bulk modulus K as :

$$K^- = K_1 + \frac{\rho_2}{\frac{1}{(K_2 - K_1)} + \frac{3\rho_2}{(3K_1 + 4G_1)}} \tag{12}$$

$$K^+ = K_2 + \frac{\rho_1}{\frac{1}{(K_1 - K_2)} + \frac{3\rho_2}{(3K_2 + 4G_2)}} \tag{13}$$

G_i is the shear modulus and K_i is the bulk modulus of the *i*-phase (EPS-phase or bacteria-phase) and they are expressed respectively as follows :

$$G_i = \frac{E_i}{2(1+\nu_i)} \tag{14}$$

$$K_i = \frac{E_i}{3(1-2\nu_i)} \tag{15}$$

Finally, we can define the effective elastic moduli bounds:

$$E^- = \frac{9K^-G^-}{(3K^- + G^-)} \tag{16}$$

$$E^{+} = \frac{9K^{+}G^{+}}{(3K^{+} + G^{+})} \tag{17}$$

These both analytical solutions are used as reference solutions in order to validate the current approach and to highlight the influence of the spatial structure on mechanical properties. In our case, the bacteria are more rigid than the EPS matrix. Indeed, some studies have shown that bacteria have a certain stiffness in particular thanks to their membranes (Alonso-Hernando *et al.* 2010; Najjar *et al.* 2007; Kudoyarov *et al.* 2011). On the contrary, EPS matrices are known to be highly hydrated (near 97 % of EPS mass is water) (Beveridge 1988) and consequently present a low stiffness, which can also change according to the presence of cations and/or other environmental parameters. The lower Hashin and Shtrikman bound corresponds to the case where the inclusions are more rigid than the matrix. The bound E^{-} is therefore expected to be the closest to our simulations.

2.7 Shear test for the study of the biofilm detachment

The accumulation of microorganisms on surfaces and biofilm development is recognized as a major strategy of microbial survival in natural and artificial environments. This accumulation is the balance of attachment, growth and detachment processes (Costerton *et al.* 1995; Costerton and Stewart 2001). Detachment may be defined as the transport of bacterial particles from the attached biofilm phase to the fluid phase. The detachment process occurs when external forces are larger than the internal strength of the matrix (Horn *et al.* 2003). These forces can be of several types including the following: fluid dynamic forces, shear forces, lift and taxis.

Real loadings are very complex, and primarily depend on the hydrodynamics, geometry and mechanical properties of the biofilm (Chang *et al.*, 1991 Stoodley *et al.* 1999a). For simplicity, our study is based on a simplified model of wall shear stress. In order to simulate hydrodynamic loadings, we apply suitable boundary conditions on the edge of the whole biofilm with periodic conditions on lines 1 and 3 (Figure 5):

$$\begin{cases} u_1(l_2) = u_2(l_2) = u_2(l_4) = 0 \\ u_1(l_4) = \alpha \\ u_1(l_1) = u_1(l_3) \\ u_2(l_1) = u_2(l_3) \end{cases} \tag{18}$$

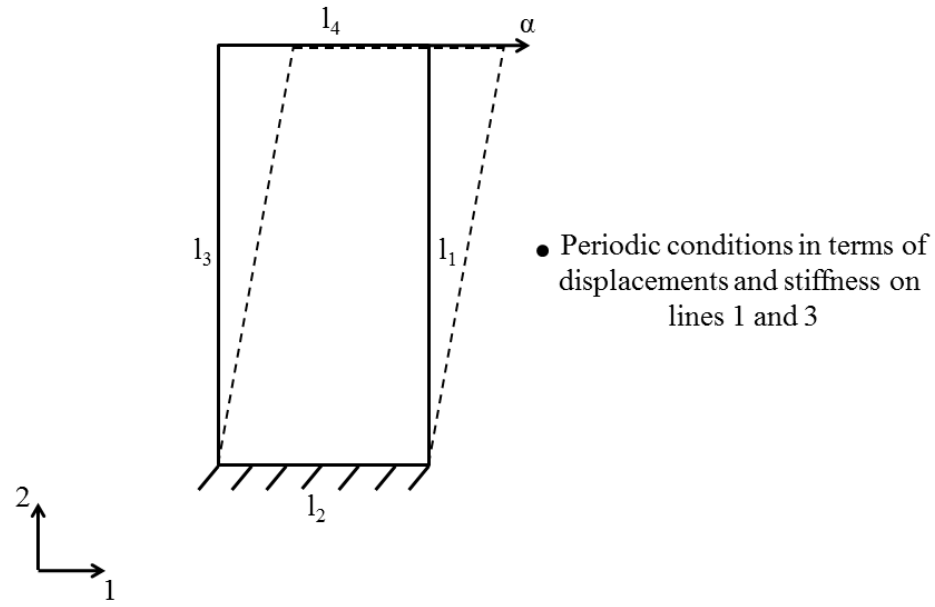

Figure 5: Boundary conditions for the wall shear stress test. We can see the deformed shape of the biofilm when it is subjected to a hydrodynamic loading.

We consider that the biofilm has homogenized properties (E_h and ν_h) within the 12 RVE (Figure 8). We have calculated the coefficient of variation (β) of the homogenized stiffness following the *x*-direction in the biofilm. The maximum value of β is equal to 0.194 enabling us to assume that variations in stiffness are not significant along the *x*-direction. It enables us to have periodic conditions on lines 1 and 3 in terms of displacements and stiffness and therefore check Equation 18. Results are presented in Table 1.

	Image 1	Image 2	Image 3	Image 4
Zone 4 (Top)	E_{moy} = 1.456 Pa ν_{moy} =0.249 β = 0.085	E_{moy} = 1.59 Pa ν_{moy} =0.240 β = 0.151	E_{moy} = 1.535 Pa ν_{moy} =0.298 β = 0.194	E_{moy} = 2.095 Pa ν_{moy} =0.272 β = 0.130
Zone 3 (Middle top)	E_{moy} = 2.740 Pa ν_{moy} =0.275 β = 0.053	E_{moy} = 2.820 Pa ν_{moy} =0.404 β = 0.143	E_{moy} = 2.192 Pa ν_{moy} =0.177 β = 0.081	E_{moy} = 3.381 Pa ν_{moy} =0.251 β = 0.074
Zone 2 (Middle bottom)	E_{moy} = 2.454 Pa ν_{moy} =0.307 β = 0.114	E_{moy} = 3.591 Pa ν_{moy} =0.438 β = 0.122	E_{moy} = 2.577 Pa ν_{moy} =0.325 β = 0.126	E_{moy} = 4.382 Pa ν_{moy} =0.336 β = 0.077
Zone 1 (Bottom)	E_{moy} = 3.375 Pa ν_{moy} =0.223 β = 0.028	E_{moy} = 3.728 Pa ν_{moy} =0.204 β = 0.055	E_{moy} = 3.347 Pa ν_{moy} =0.104 β = 0.031	E_{moy} = 4.905 Pa ν_{moy} =0.186 β = 0.038

Table 1: Coefficient of variation (β) of the homogenized rigidity calculated in the x-direction according to the y-direction.

3 Results and discussion

3.1 RVE study

As explained in section 2.3, the choice of the RVE size constitutes a key issue due to the difficulty to define the representativeness of the volume. In order to determine a relevant RVE, we performed a convergence study investigating the variation of the homogenized parameter E_h according to different RVE sizes. The selected experimental sizes of RVE are represented in Figure 6.

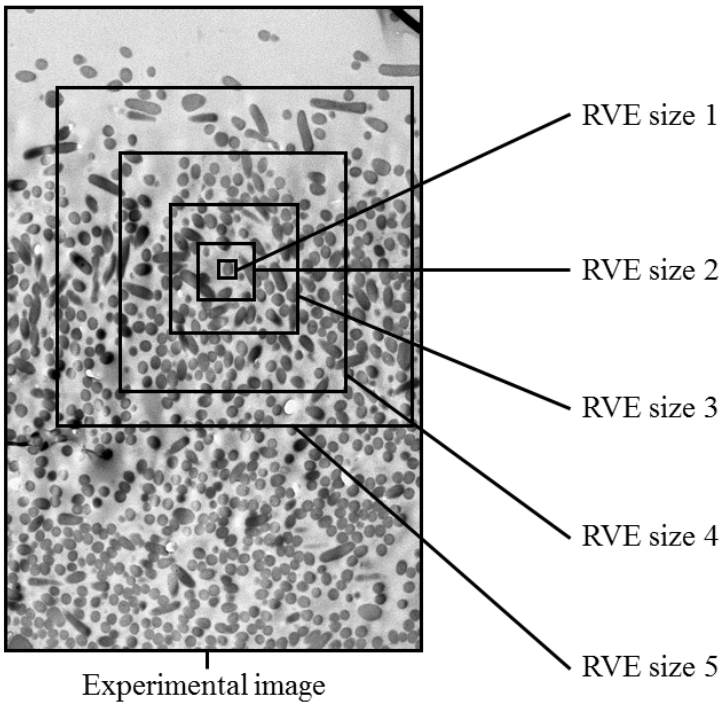

Figure 6: Convergence study performed on several RVE sizes. It allows us to define a suitable RVE size in order to apply homogenization technique.

The convergence curve is shown in Figure 7. The different RVE sizes are: RVE 1: $1\mu m \times 1\mu m$, RVE 2: $5\mu m \times 5\mu m$, RVE 3: $10\mu m \times 10\mu m$, RVE 4: $20\mu m \times 20\mu m$ and RVE 5: $40\mu m \times 40\mu m$. For the calculation of the homogenized stiffness, we used : E_b=100 Pa and E_m=1 Pa. There is a ratio of 100 between the values of the matrix stiffness because we suppose that the stiffness of the bacteria is much higher as explained in section 2.6. The influence of this ratio is analyzed in section 3.3.

The calculation of the homogenized stiffness is performed on the five different RVE sizes. The “min/max” bar corresponds to the minimum and the maximum values of the different computations of the homogenized stiffness. For each size of RVE, we have calculated the homogenized stiffness on several replicates. In Figure 7, for each RVE size, we have represented the minimum and the maximum values and the mean of homogenized stiffness of all replicates. Also note that, at the bottom of the biofilm, where the number of bacteria is high, the convergence is faster. If the minimum and maximum values are close, all RVE lead to the same result. In this case, we can conclude that the RVE has a good representativeness. As shown on Figure 7, the "min/max" bar is very significant for small surfaces of RVE, and decreases with respect to the RVE surface. The mean value converges for a RVE area greater than 200 μm^2. With this spatial structure, we can conclude that a domain with a size of 15 µm by 15 µm is

representative in terms of mechanical functions, independent of the location. This convergence analysis has been performed on multiple experimental images with similar results (data not shown).

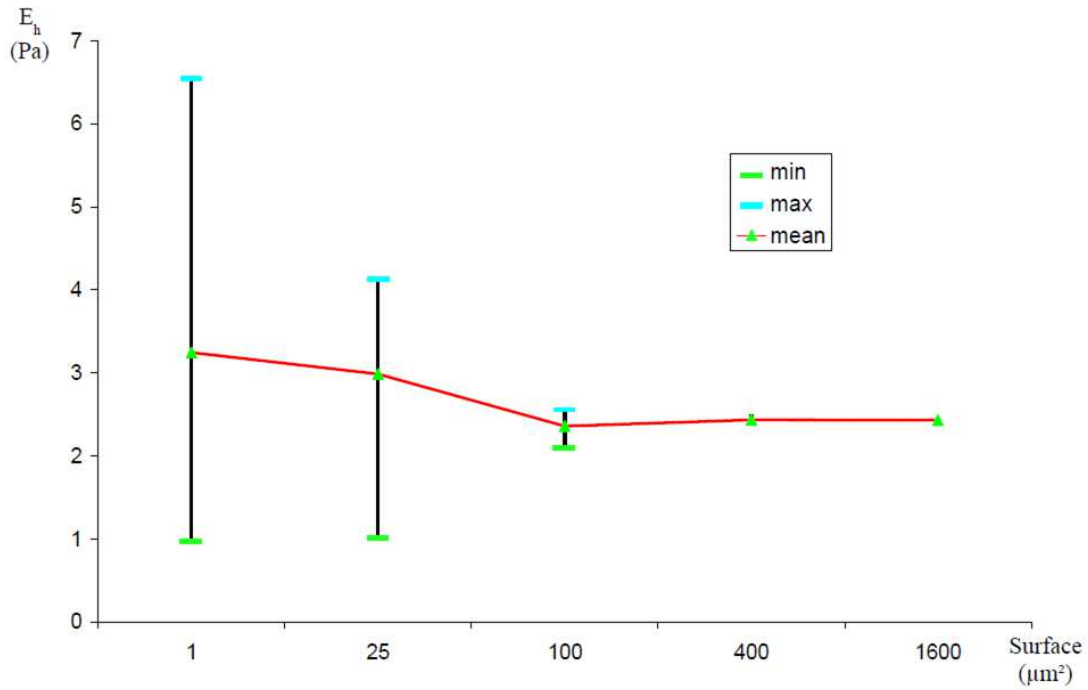

Figure 7: Calculation of the homogenized parameter according to the RVE size. There is a high degree of dispersion (high gap between the minimum and the maximum values of the homogenized rigidity calculated from several replicates) for small surfaces of RVE. For each RVE size, the triangle represents the mean of the homogenized stiffness calculated from all replicates.

3.2 Stiffness map of the biofilm

Once the RVE convergence was determined, the RVE was moved following a pitch equal to 15 µm in both 1- and 2- directions. Homogenization techniques (described above) were then applied to the twelve RVE that are distinguishable in Figure 8a. For the calculation of the homogenized stiffness, the RVE is a square of side 15 µm and we always used: E_b =100 Pa and E_m =1 Pa.

The homogenization results are also shown on Figure 8. The stiffness map is plotted with the four biofilm experimental images (Figure 8b). All images present similar characteristics. Indeed, there is a high degree of stiffness variation throughout the biofilm. The maps clearly show stiffness heterogeneities, which can be partially explained by the bacterial distribution throughout the biofilm. For example, the bottom corresponds to the beginning of the biofilm formation

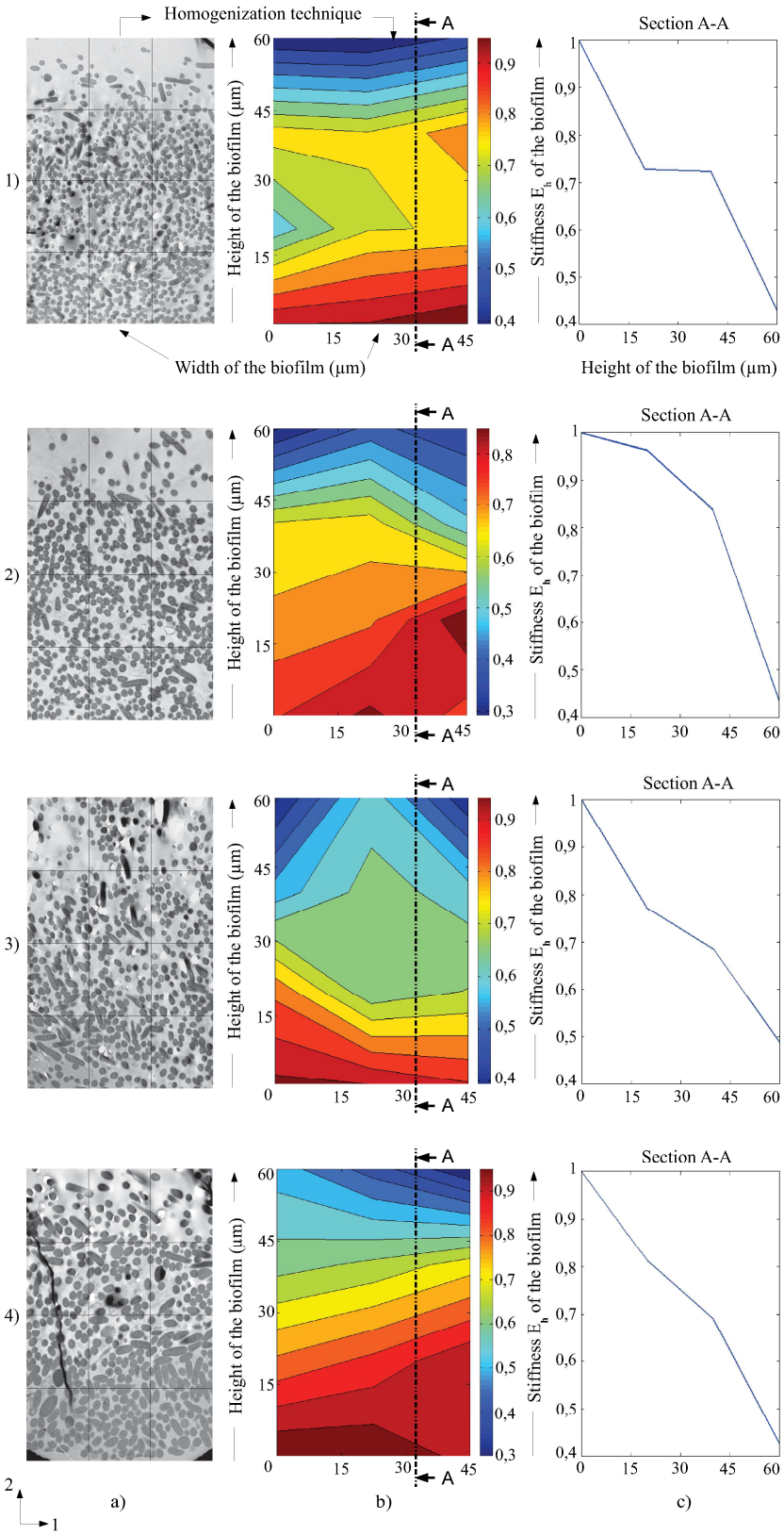
Homogenization technique
A
Section A-A
1)
2)
3)
4)
Height of the biofilm (µm)
Width of the biofilm (µm)
Stiffness E_h of the biofilm
Height of the biofilm (µm)
2
1
a)
b)
c)

Figure 8

Figure 8: Rigidity maps of biofilm experimental images. a) The whole biofilm is discretized in 12 RVE. b) The rigidity map and c) the mean section are plotted to investigate the evolution of the rigidity into the biofilm.

leading to a dense cell packing order due to a high substrate concentration. The stiffness is therefore the highest. On the contrary, at the top of the biofilm, close to the biofilm-media interface there is a structure with few scattered bacteria, leading to a lower stiffness. This low number of bacteria at the top may be explained by several phenomena such as hydrodynamic stress, shear forces or cell-cell interactions. In this case, the stiffness is less significant. This study clearly demonstrates that the stiffness variations strongly depend on three issues: the bacterial spatial distribution, the volume fraction of the two phases and the values of microscopic parameters, E_m and ν_m for the EPS matrix, E_b and ν_b for the bacteria. In the mean sections shown in Figure 8c, there are clearly two abrupt variations of stiffness, indicating that the mechanical properties rapidly change at the top and at the bottom of the biofilm. In Figure 9, we can see the evolution of the homogenized stiffness according to the biofilm height and we can compare the numerical results with the analytical results. In Figure 9a, we can note that the numerical results ranged between the Hashin and Shtrikman bounds. This result confirms what it was expected, *i.e.* the numerical calculations are very close to the lower bound of Hashin and Shtrikman E^- because bacteria are more rigid than the EPS matrix. Moreover, the results fit the previous conclusions, i.e., at the bottom, the high number of bacteria participates to have a higher stiffness. On the contrary, at the top, the low number of the bacteria contributes to a lower stiffness. We can also note that the gap varies between the numerical result and the lower bound E^- within the biofilm (see Figure 9b).

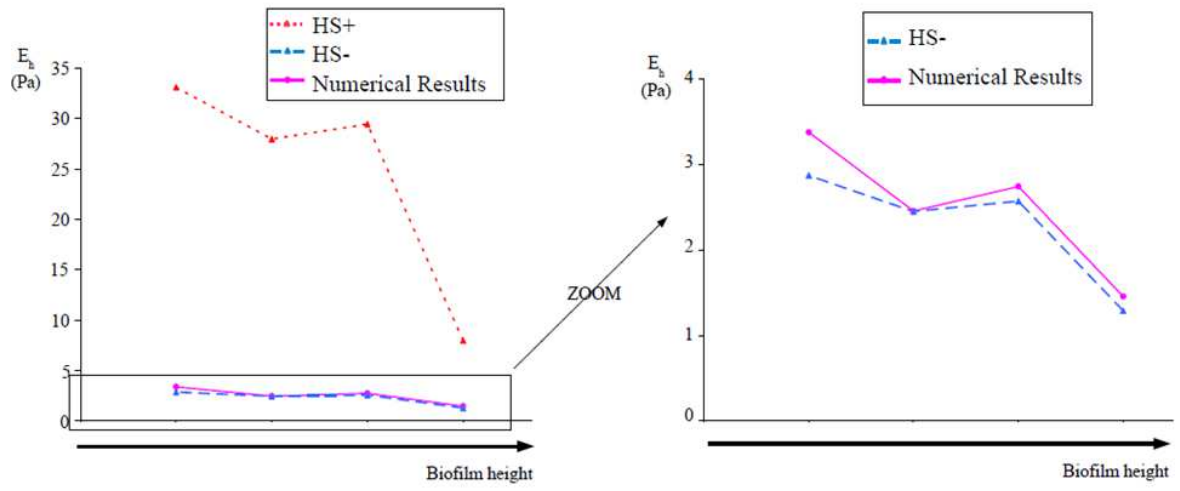

Figure 9: Comparison between numerical results and analytical solution of Hashin and Shtrikman a). We can also note that the gap between the numerical results and the lower bound of Hashin of the homogenized rigidity varies according to the locations of the biofilm due to a little orthotropic effect, to the spatial structure and to the bacteria shapes b).

Many reasons may be explain this difference. We hypothesize that the biofilm has an elastic isotropic behaviour at the microscope scale. In order to assume this hypothesis, we carried out the same study but we consider that the biofilm has an orthotropic behaviour. The energetic based technique was therefore used in the orthotropic case (not detailed here for the sake of simplicity). The energy based technique allowed us to compute the homogenized stiffness in the 1- and 2-directions respectively. In order to characterize the orthotropic effect, we calculated the orthotropic coefficient r which corresponds to the ratio between these two values:

$$r = \frac{E_2}{E_1} \tag{19}$$

The mean of this coefficient is equal to 0.95, which supports the isotropic approximation but can also explain a part of the gap between numerical and analytical results. On the other hand, the spatial structure of the biofilm and the shape of the bacteria can explain this difference. Indeed, the spatial structure is not uniform and the bacteria have various shapes such as spherical, oval or little stick, which may influence the results.

3.3 Sensitivity analysis of the ratio of microscopic stiffness

As explained above, we suppose that the bacterial stiffness is higher than the EPS matrix stiffness but it is very difficult to quantify the difference. In order to analyse the influence of these microscopic values, we perform a sensitivity analysis on the ratio of the microscopic parameters (E_m/E_b). We compute the homogenized stiffness E_h for four different values of E_m(1;10;30;50) leading to four values of the ratio E_m/E_b (0.01;0.1;0.3;0.5) according to the bacterial distribution of the biofilm. On Figure 10, we investigate the influence of this ratio on homogenized stiffness in four locations throughout the biofilm. The locations were selected at different heights from zone 1 at the bottom to zone 4 at the top. We show that the homogenized stiffness evolves almost linearly with the ratio at the top of the biofilm. Indeed, the number of bacteria at the top is low, and the homogenized stiffness is proportional to the value of the matrix stiffness E_m and therefore to the ratio E_m/E_b. Then, the evolution of the homogenized stiffness clearly tends to be more nonlinear when the location in the biofilm is close to the substratum, where the number of bacteria is high. This approach allows us to see the high sensitivity of the microscopic parameters of the stiffness. The factor between both values may be very large and strongly impact the values of the stiffness. As explained above, the values of the stiffness of the EPS matrix are most probably lower than the stiffness of the bacteria due to the fact that EPS matrix is highly hydrated. But, the percentage of water in EPS matrix may play a major role in the final value of EPS stiffness.

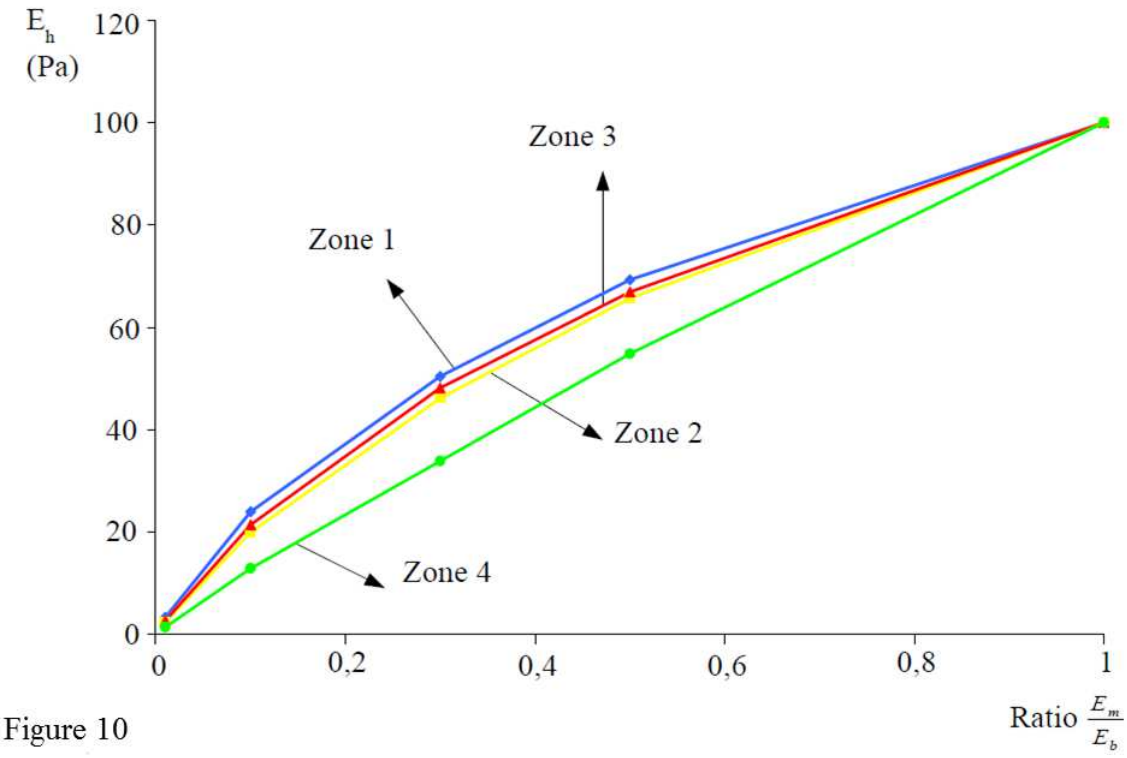

Figure 10

Figure 10: Influence of the ratio $\frac{E_m}{E_b}$ on homogenized rigidity at different locations of the biofilm. The nonlinearity increases when the biofilm height increases.

3.4 Influence of the stiffness distribution on the biofilm detachment

We also assessed the influence of the stiffness spatial variations on the biofilm detachment by simulating a hydrodynamics test (as explained in section 2.7). Many studies in fracture mechanics are based on energetic criteria, so we have therefore decided to use an energetic criterion to define zones where the detachment is the most probable. For this purpose, we compute the local strain energy *W* within each zone according to the characteristic E_h and ν_h of each homogenized RVE. For a sake of clarity, values of strain energy *W* are normalized according to the highest value of the strain energy and are denoted $\tilde{W}$ in order to compare detachment between biofilms. In zones where the strain energy $\tilde{W}$ is superior to $\tilde{W}_{limit}$, detachment has a high probability to occur. In contrast, there is a low probability of detachment in zones where $\tilde{W}$ is inferior to $\tilde{W}_{limit}$,. To determine detachment locations, we choose $\tilde{W}_{limit} = 0.6$. The strain energy map, the detachment mode and the locations where the probability of detachment is the highest are represented in Figure 11. Experimental image maps clearly show variations in strain energy due to variations of stiffness according to the *2*-direction. The detachment zones are colored in grey

on Figure 11. These zones correspond to two types of detachment:

- erosion: detachment occurs at the top of the biofilm close to the fluid/biofilm interface (Figure 11,a-d). It leads to the detachment of few bacteria or small fragments of the biofilm. Erosion is basically a surface process. The wall shear stress causes the detachment of single cell or small portion of the biofilm at the fluid / biofilm interface (Bryers 1988);

- sloughing: occurs within the biofilm where the bacteria density decreases. Generally, it leads to the detachment of large parts of the biofilm (Bryers 1988; Ohashi and Harada 1994b). We can distinguish two different sloughing cases. Sloughing can occur near the middle of the biofilm (Figure 11a). In this case, this detachment can be associated with a cohesive failure. The second type of sloughing occurs at the bottom of the biofilm, close to the biofilm/substrate interface. In this case, sloughing may result in the entire biofilm detaching (Figure 11c) and can be associated with an adhesive failure. Note that if we want to quantify the adhesive failure, a more refined model has to be used by considering the interfacial model between the biofilm and the substrate.

Furthermore, we plotted the distributions of the strain energy according to the *2*-direction (along the height of the biofilm). It enables us to locate the different detachment zones: erosion, sloughing with cohesive failure and sloughing with adhesive failure. It clearly shows that the detachment mode is strongly linked to stiffness heterogeneities within the biofilm.

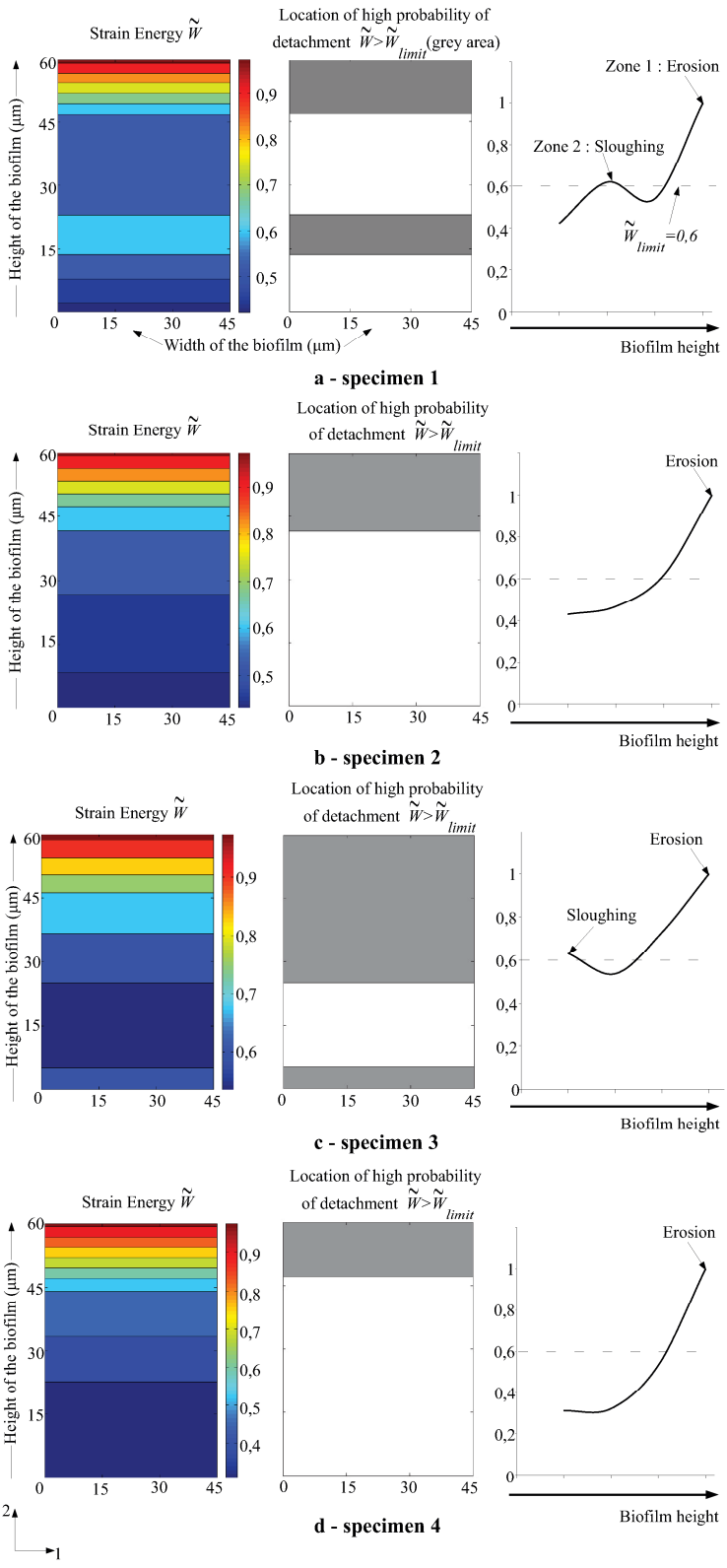
Strain Energy $\tilde{W}$
Location of high probability of detachment $\tilde{W}>\tilde{W}_{limit}$ (grey area)
Height of the biofilm (µm)
Width of the biofilm (µm)
Zone 1 : Erosion
Zone 2 : Sloughing
$\tilde{W}_{limit}$=0,6
Biofilm height
a - specimen 1
Location of high probability of detachment $\tilde{W}>\tilde{W}_{limit}$
Erosion
b - specimen 2
c - specimen 3
Sloughing
d - specimen 4
2
1

Figure 11

Figure 11: Influence of rigidity distribution on biofilm detachment. The whole biofilm is discretized in 12 homogenized RVE, transformed in four levels due to the periodic conditions and the map of the strain energy is plotted. We can see the mode of the detachment and the location where it has the highest probability to occur.

4 Conclusion

Novel experimental methods create new opportunities to carry out analyses of mechanical properties within bacterial biofilms. Here, we use an original experimental approach; freeze-substitution electron microscopy coupled with a homogenization procedure in order to study biofilm mechanics in a single-species biofilm. This coupling allows us to show that bacterial distribution leads to significant stiffness heterogeneities within the biofilm which may partly explain the detachment phenomena. Moreover, it explains the different detachment modes observed in the literature such as erosion or sloughing. In the future, we intend to use of a more complex mechanical models such as interfacial models which will allows us to analyse biofilm failures and more complex natural microbial communities.

References

Aboudi, J. (1991) Mechanics of composite materials - A unified micromechanical approach.

Aggarwal, S., Hozalski, R. (2010) Determination of biofilm mechanical properties from tensile tests performed using a micro-cantilever method. Biofouling, 26(4):479-486.

Aggarwal, S., Poppele, E., Hozalski, R. (2010) Development and testing of a novel microcantilever technique for measuring the cohesive strength of intact biofilms. Biotechnology and Bioengineering, 105(5):924-934.

Allesen-Holm, M., Barken, K., Yang, L., Klausen, M., Webb, J., Kjelleberg, S., Molin, S., Givskov, M., Tolker-Nielsen, T. (2006) A characterization of dna release in pseudomonas aeruginosa cultures and biofilms. Molecular Microbiology, 59(4):1114-1128.

Alonso-Hernando, A., Alonso-Calleja, C., Capita, R. (2010) Effects of exposure to poultry chemical decontaminants on the membrane fluidity of listeria monocytogenes and salmonella enterica strains. International Journal of Food Microbiology, 137(2-3):130-136.

Beech, I., Sunner, J. (2004) Biocorrosion: Towards understanding interactions between biofilms and metals. Current Opinion in Biotechnology, 15(3):181-186.

Bryers, J. (1988) Modeling biofilm accumulation. In: Bazin M, Prosser JI, Editors. Physiological models in microbiology. Boca Raton, FL: CRC Press. p 109-144.

Beveridge, T. J. (1988) Wall ultrastructure; how little we know, p. 3–20. In P. Actor, L. Daneo-Moore, M. L. Higgins, M. R. J. Salton, and G. D. Shockman (ed.), Antibiotic inhibition of bacteria cell surface assembly and function. ASM Press, Washington, D.C.

Cense, A., Van Dongen, M., Gottenbos, B., Nuijs, A., Shulepov, S. (2006) Removal of biofilms by impinging water droplets. Journal of Applied Physics, 100(12).

Chang, H. (1983) Effective diffusion and conduction in two-phase media: a unified approach. AIChE Journal, 29:846-853.

Chang, H.T., Rittmann, B.E., Amar, D., Heim, R., Ehlinger, O., Lesty, Y. (1991) Biofilm detachment mechanisms in a liquid-fluidized bed, Biotechnology and Bioengineering, 38(5):499-506.

Chen, M., Zhang, Z., Bott, T. (1998) Direct measurement of the adhesive strength of biofilms in pipes by micromanipulation. Biotechnology Techniques, 12(12):875-880.

Chen, M., Zhang, Z., Bott, T. (2005) Effects of operating conditions on the adhesive strength of pseudomonas fluorescens biofilms in tubes. Colloids and Surfaces B: Biointerfaces, 43(2):61-71.

Coetser, S., Cloete, T. (2005) Biofouling and biocorrosion in industrial water systems. Critical Reviews in Microbiology, 31(4):213-232.

Costerton, J., Lewandowski, Z., Caldwell, D., Korber, D., Lappin-Scott, H. (1995) Microbial biofilms. Annual Review of Microbiology, 49:711-745.

Costerton, J., Stewart, P. (2001) Battling biofilms. Scientific American, 285(1):74-81.

Coufort, C., Derlon, N., Ochoa-Chaves, J., Liné, A., Paul, E. (2007) Cohesion and detachment in biofilm systems for different electron acceptor and donors. Water Science and Technology, 55(8-9):421-428.

De Beer, D., Stoodley, P. (1995) Relation between the structure of an aerobic biofilm and transport phenomena. Water Science and Technology, 32(8):11-18.

De Beer, D., Stoodley, P., Roe, F., Lewandowski, Z. (1994) Effects of biofilm structures on oxygen distribution and mass transport. Biotechnology and Bioengineering, 43(11):1131-1138.

Dormieux, L., Molinari, A., Kondo, D. (2002) Micromechanical approach to the behaviour of poroelastic materials. Journal of the Mechanics and Physics of Solids, 50(10):2203-2231.

Fritsch, A., Dormieux, L., Hellmich, C., Sanahuja, J. (2009) Mechanical behavior of hydroxyapatite biomaterials: An experimentally validated micromechanical model for elasticity and strength. Journal of Biomedical Materials Research - Part A, 88(1):149-161.

Godon, J.-J., Zumstein, E., Dabert, P., Habouzit, F., Moletta, R. (1997) Molecular microbial diversity of an anaerobic digestor as determined by small-subunit rdna sequence analysis. Applied and Environmental Microbiology, 63(7):2802-2813.

Guélon, T., Mathias, J.D., Stoodley, P. (2011) Advances in biofilm mechanics, H.-C. Flemming et al. (eds.), Biofilm Perspectives, Springer Series on Biofilms 5.

Guélon, T., Mathias, J.-D., Deffuant, G., (2012) Influence of spatial structure on effective nutrient diffusion in bacterial biofilms, Journal of Biological Physics, (in Press).

Hashin, Z. (1983) Analysis of composite materials - a survey. Journal of Applied Mechanics, Transactions ASME, 50(3):481-505.

Hashin, Z., Shtrikman, S. (1963) A variational approach to the theory of the elastic behaviour of multiphase materials. Journal of the Mechanics and Physics of Solids, 11(2):127-140.

Hashin, Z. (1962) The Elastic Moduli of Heterogeneous Materials, Journal of Applied Mechanics (29): 143-150.

Horn, H., Reiff, H., Morgenroth, E. (2003) Simulation of growth and detachment in biofilm systems under defined hydrodynamic conditions. Biotechnology and Bioengineering, 81(5):607-617.

Hunter, R., Beveridge, T. (2005) High-resolution visualization of pseudomonas aeruginosa pao1 biofilms by freeze-substitution transmission electron microscopy. Journal of Bacteriology, 187(22):7619-7630.

Klapper, I., Rupp, C., Cargo, R., Purvedorj, B., Stoodley, P. (2002) Viscoelastic fluid description of bacterial biofilm material properties. Biotechnology and Bioengineering, 80(3):289-296.

Korstgens, V., Flemming, H.-C., Wingender, J., Borchard, W. (2001) Uniaxial compression measurement device for investigation of the mechanical stability of biofilms. Journal of Microbiological Methods, 46(1):9-17.

Kudoyarov, M., Vishnevskii, B., Manicheva, O., Myakotina, E., Mukhin, S., Patrova, M., Vedmetskii, Y. (2011) Possibilities of sterilization by track membranes. Technical Physics Letters, 37(9):881-883.

Laspidou, C., Aravas, N. (2007) Variation in the mechanical properties of a porous multi-phase biofilm under compression due to void closure. Water Science and Technology, 55(8-9):447-453.

Laspidou, C., Rittmann, B., Karamanos, S. (2005) Finite element modelling to expand the umcca model to describe biofilm mechanical behavior. Water Science and Technology, 52(7):161-166.

Lau, P., Dutcher, J., Beveridge, T., Lam, J. (2009) Absolute quantitation of bacterial biofilm adhesion and viscoelasticity by microbead force spectroscopy. Biophysical Journal, 96(7):2935-2948.

Marsh, P., Bradshaw, D. (1995) Dental plaque as a biofilm. Journal of Industrial Microbiology, 15(3):169-175.

Mathias, J.-D., Stoodley, P. (2009) Applying the digital image correlation method to estimate the mechanical properties of bacterial biofilms subjected to a wall shear stress. Biofouling, 25(8):695-703.

Michel, J., Moulinec, H., Suquet, P. (1999) Effective properties of composite materials with periodic microstructure: A computational approach. Computer Methods in Applied Mechanics and Engineering, 172(1-4):109-143.

Mori, T., Tanaka, K., (1973) Average stress in matrix and average elastic energy of materials with misfitting inclusions. Acta Metall. (21):571–574.

Najjar, M., Chikindas, M., Montville, T. (2007) Changes in listeria monocytogenes membrane fluidity in response to temperature stress. Applied and Environmental Microbiology, 73(20):6429-6435.

Ohashi, A., Harada, H. (1994a) Adhesion strength of biofilm developed in an attached-growth reactor. Water Science and Technology, 29(10-11):281-288.

Ohashi, A., Harada, H. (1994b) Characterization of detachment mode of biofilm developed in an attached-growth reactor. Water Science and Technology, 30(11):35-45.

Ohashi, A., Harada, H. (1996) A novel concept for evaluation of biofilm adhesion strength by applying tensile force and shear force. Water Science and Technology, 34(5-6 -6 pt 3):201-211.

Poppele, E., Hozalski, R. (2003) Micro-cantilever method for measuring the tensile strength of biofilms and microbial flocs. Journal of Microbiological Methods, 55(3):607-615.

Reuss, A. (1929) Berechnung des fliessgrense von mischkritallen auf grund des plastizitatsbedingung fur einkristalle. Zeitschrift fur Angewandte Mathematik und Mechanik, 9:49-58.

Rieu, A., Briandet, R., Habimana, O., Garmyn, D., Guzzo, J., Piveteau, P. (2008) Listeria monocytogenes egd-e biofilms: No mushrooms but a network of knitted chains. Applied and Environmental Microbiology, 74(14):4491-4497.

Rochex, A., Godon, J.-J., Bernet, N., Escudié, R. (2008) Role of shear stress on composition, diversity and dynamics of biofilm bacterial communities. Water Research, 42(20):4915-4922.

Socransky, S., Haffajee, A. (2002) Dental biofilms: Difficult therapeutic targets. Periodontology 2000, 28(1):12-55.

Stoodley, P., Cargo, R., Rupp, C., Wilson, S., Klapper, I. (2002) Biofilm material properties as related to shear-induced deformation and detachment phenomena. Journal of Industrial Microbiology and Biotechnology, 29(6):361-367.

Stoodley, P., Hall-Stoodley, L., Lappin-Scott, H. (2001) Detachment, surface migration, and other dynamic behavior in bacterial biofilms revealed by digital time-lapse imaging. Methods in Enzymology, 337:306-319.

Stoodley, P., Lewandowski, Z., Boyle, J.D., Lappin-Scott, H. (1999a) Structural deformation of bacterial biofilms caused by short-term fluctuations in fluid shear: An in situ investigation of biofilm rheology. Biotechnology and Bioengineering, 65(1):83-92.

Stoodley, P., Lewandowski, Z., Boyle, J., Lappin-Scott, H. (1999b) The formation of migratory ripples in a mixed species bacterial biofilm growing in turbulent flow. Environmental microbiology, 1(5):447-455.

Suquet, P., (Ed.), 1997. Continuum micromechanics, CISM Lecture notes, Udine, Italy, Springer-Verlag, Berlin.

Voigt, W. (1889) Uber die beziehung zwischen den beiden elasticitatsconstanten isotroper korper. Annalen des Physik (Leipzig), 38:573-587.

Wagner, M., Loy, A. (2002) Bacterial community composition and function in sewage treatment systems. Current Opinion in Biotechnology, 13(3):218- 227.

Wood, B., Whitaker, S. (1998) Diffusion and reaction in biofilms. Chemical Engineering Science, 53(3):397-425.

Wood, B., Whitaker, S. (1999) Cellular growth in biofilms. Biotechnology and Bioengineering, 64(6):656-670.

Woolard, C., Irvine, R. (1994) Biological treatment of hypersaline wastewater by a biofilm of halophilic bacteria. Water Environment Research, 66(3):230-235.

Xavier, J., Martinez-Garcia, E., Foster, K. (2009) Social evolution of spatial patterns in bacterial biofilms: When conflict drives disorder. American Naturalist, 174(1):1-12.